01 Jan 1992

°-Electron Emission In Fast Heavy Ion Atom Collisions

H. Schmidt-Böcking

U. Ramm

G. Kraft

J. Ullrich

et. al. For a complete list of authors, see https://scholarsmine.mst.edu/phys_facwork/2599

Recommended Citation

H. Schmidt-Böcking and U. Ramm and G. Kraft and J. Ullrich and H. Berg and C. Kelbch and R. E. Olson and R. D. DuBois and S. Hagmann and F. Jiazhen, "°-Electron Emission In Fast Heavy Ion Atom Collisions," *Advances in Space Research*, vol. 12, no. 2 thru 3, pp. 7 - 15, Elsevier, Jan 1992.
The definitive version is available at https://doi.org/10.1016/0273-1177(92)90084-B

Adv. Space Res. Vol. 12, No. 2–3, pp. (2)7–(2)15, 1992
Printed in Great Britain.

0273–1177/92 $15.00

δ-ELECTRON EMISSION IN FAST HEAVY ION ATOM COLLISIONS

H. Schmidt-Böcking,* U. Ramm,* G. Kraft,** J. Ullrich,**
H. Berg,* C. Kelbch,* R. E. Olson,*** R. DuBois,† S. Hagmann‡
and F. Jiazhen*

* *Institut für Kernphysik, Universität Frankfurt, D-6000 Frankfurt/Main, Germany*
** *GSI, D-6100 Darmstadt 11, Germany*
*** *Physics Department, University of Missouri-Rolla, Rolla, MO 65401, U.S.A.*
† *Pacific Northwest Laboratory, Richland, WA 99352, U.S.A.*
‡ *Physics Department, Kansas State University, Manhattan, KS 66506, U.S.A.*

ABSTRACT

Biological damages such as mutations, chromosomal aberrations etc. are a consequence of biochemical changes mostly in the DNA /1/. With ionizing radiation, these chemical changes are due to primary ionization events and secondary ionization effects caused by the primarily produced electrons.

Differences in the biological response of densely ionizing radiation, like heavy charged particles, in comparision to sparsely ionizing radiation, such as X- or γ-rays, are mainly due to the differences in the production of the so called δ-electrons. Therefore, the emission process of electrons i.e. the cross section for the primary ionization event as well as the energy and angular distribution of the emitted electrons should be understood in detail.

The δ-electron emission processes occuring in fast heavy ion atom collisions are explained qualitatively. The different spectral structures of electron emission arising from either the target or the projectile are explained in terms of simple models of the kinetics of momentum transfer induced by the *COULOMB* forces.

In collisions of very heavy ions with matter, high nuclear *COULOMB* forces are created. These forces lead to a strong polarization of the electronic states of the participated electrons. The effects of this polarization are discussed.

INTRODUCTION

Fast ions penetrating matter interact via *COULOMB* forces mainly with the target electrons. Thus the target atoms are excited and ionized after the collision. The continuous kinetic energy (E_e) and angular distribution (ϑ_e) of the emitted δ-electrons are superimposed by several discrete lines. In Figure 1 typical energy spectra for δ-electrons resulting from heavy ion impact on a gas target are shown /2/. Measurements were performed at different angles. The brackets [1] to [5] indicate important electron emission processes at different energies. These processes are the following:

[1] the continous three body δ-electron emission and
[2] the two body δ-electron emission,
[1] and [2] both result from target ionization;

[3] Auger-electron emission of the multiply excited target atom;
[4] projectile Auger-electron emission,
[3] and [4] both result from inner shell autoionization processes and

[5] electron loss from the projectile.

In the following, these five processes will be discussed in detail.

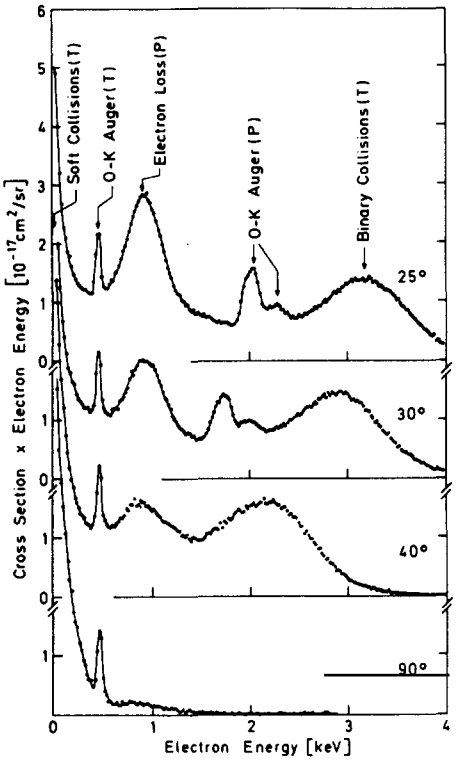

Fig. 1. Cross section times electron energy for electron production in $30 - MeV\ O^{5+} + O_2$ Collisions at different electron observation angles (from /2/).

ELECTRON EMISSION PROCESSES

Two and three body interaction

To understand the most important contributions, process [1] and [2], the kinematic of the electron emission process and the momentum transfer (i.e. cross section) have to be considered. In Figure 2, a scheme of the collision processes is presented. It is assumed that the charged projectile has a straight line trajectory. Then the two impact parameters b_N (projectile-target nucleus distance of closest approach) and b_e (projectile-electron distance of closest approach), and the electron-target nucleus distance vector ($\vec{r}_e$) characterize the interacting *COULOMB* forces.

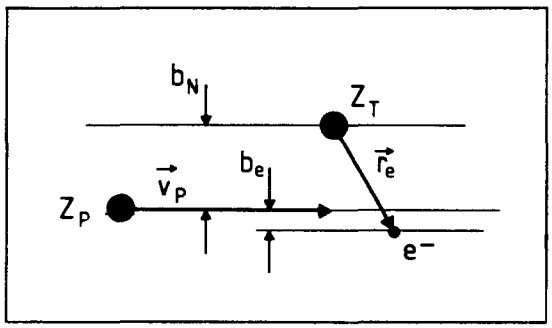

Fig. 2. Scheme of the collision processes.

In the first case the projectile-electron impact parameter b_e is given to be smaller than the projectile-target nucleus impact parameter b_N. Since the *COULOMB* forces decrease with $1/(distance)^2$, for $b_e \ll b_N$ the ionizing interaction between the target nucleus and the target electron can be neglected. Thus the ionization mechanism can be explained classically as a two body collision process between the projectile and the target electron (process [2]): the δ-electrons are originated from a so called *BINARY ENCOUNTER* (*BE*).

In Figure 3a the classical trajectories are displayed with the initial and the final momenta $\vec{p}_j^{\,i,f} = m_j \vec{v}_j^{\,i,f}$ in the laboratory-system (*LS*) indicating the momentum exchange in this classical two body collision process. Initially, the target electron is assumed as quasifree and motionless. Accordingly, for the emitted *BE*-electrons we obtain a simple E_e-ϑ_e-relationship:

$$E_e^{BE}(\vartheta_e) = 2m_e \vartheta_p^2 \cos^2 \vartheta_e. \tag{1}$$

In this formular at a fixed projectile velocity only one electron energy corresponds to a given emission angle. However, because of the initial electron momentum the *BE* peak is broadened around $E_e^{BE}(\vartheta_e)$ and its real peak maximum is slightly shifted to lower energies. From Equation (1) the maximum energy for the *BE*-electrons is calculated at $\vartheta_e = 0^0$ and this so called *KNOCK − ON COLLISION* creates electrons with $E_e^{BE} = 2m_e \vartheta_p^2$.

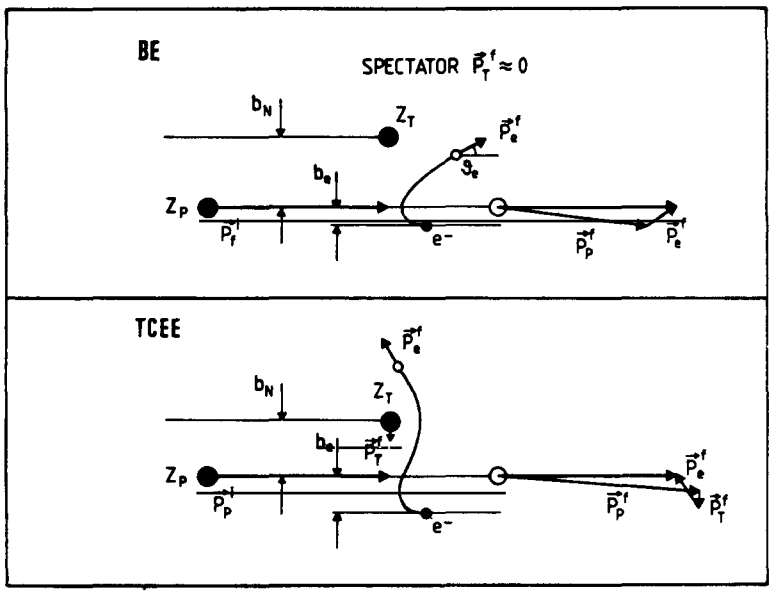

Fig. 3. Classical trajectories for the *BE* (a) and the *TCEE* (b) processes. The vectors $\vec{p}_j^{\,i,f} = m_j \vec{v}_j^{\,i,f}$ represent the initial and the final momentum vectors of the colliding particles.

Due to a classical two body collision where the mass of the electron (m_e) is very small in comparison to the mass of the projectile (m_P), the δ-electron is reflected from the projectile with twice the velocity of the projectile ($\vec{v}_P$). Because of the cos^2 emission characteristics of Formular (1) the *BE* peak disappears at emission angles of 90^0.

The biggest contribution to the δ-electron spectra (see Figure 1) is the exponentially decreasing continuum (process [1]) with its maximum at 0eV. This corresponds to a very small momentum transfer between the projectile nucleus and the target electron. Generally, the yield of these electrons exceeds the intensity of all other contributions in the spectra by orders of magnitude. They originate from the so called *SOFT – COLLISIONS* where the distances of the projectile to the target nucleus and to the target electrons are of nearly the same size ($b_e \geq b_N$, see Figure 3b). Consequently, the ionization process has to be described by a three body momentum exchange, where the initial and the final momenta of both, the projectile and the target nucleus, have a strong influence on the δ-electron emission. Within this *TWO CENTRE ELECTRON EMISSION* (*TCEE*) process, the electron is first ejected from the target atom by the interaction with the projectile. Since the *COULOMB* forces of the projectile and the target nucleus are of approximately equal strength, the electron is also scattered by the target nucleus, yielding an angular distribution, completely different from those received from *BE* emission. In contrast to the *BE*-process where mainly one energy corresponds to a definit angle, for the *TCEE*-electrons for each emission angle a continous emission spectrum is obtained.

In Figure 4 the expected angular distribution of the quantity of the *BE* and the *TCEE* process is shown schematically. The *BE*-electrons, originated from the classical two body collision process, can only be emitted between $\vartheta_e = 0^0$ and 90^0 within the laboratory-system. Because of the Rutherford scattering trajectory of the projectile-electron collision the emission angle (ϑ_e) depends on the size of the impact parameter (b_e). In the *LS* *BE*-electrons emitted to small ϑ_e result from very close collisons, the so called *KNOCK – ON COLLISION*, where b_e is small; collisions at larger b_e yield $\vartheta_e^{Lab} \longrightarrow 90^0$. Since the probability, i.e. the intensity of electron emission increases with the square of the impact parameter (b_e^2), the largest amount is observed towards 90^0.

In the case of *TCEE* processes, δ-electrons are scattered twice; once at the projectile and again at the target nucleus. Therefore, the electrons are emitted to all angles between $\vartheta_e = 0^0$ and 180^0; the angular distribution is nearly isotropic in the *LS*.

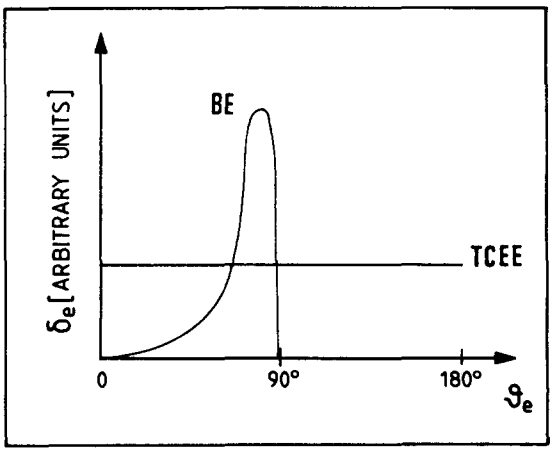

Fig. 4. Schematical presentation of the angular dependence of the *BE* and *TCEE* processes in fast light ion atom collisions.

However, we will see below, that for very heavy ion atom collisions the angular distribution of the δ-electrons from the *TCEE* can be very anisotropic too. Because of the polarization effects of electronic states due to the *COULOMB* force of the heavy projectile the δ-electrons are emitted strongly in the forward direction /3/.

Target Auger electron emission

The peak in the energy spectrum of Figure 1 labeled $O-K-AUGER\,(T)$ corresponds to autoionization of the target (process [3]), the so called *AUGER ELECTRON EMISSION PROCESS*. Autoionization follows production of vacancies in the inner shells of the target atoms. These vacancies are produced by the incident projectile via ionization or multiple excitation of the inner shells of the target atom.

In Figure 5 this emission process is shown schematically for a $KLL-AUGER$ electron; one vacancy in the K-shell and two electrons in the L-shell participate. While one of the L-shell electrons falls down into the groundstate and fills up the K-shell vacancy, the difference of the electron binding energies in both shells is transmitted to the second electron. Hence, this electron is emitted with the energy

$$E_{e,AUGER} = h\nu_{K_\alpha} - E_L = E_K - 2E_L. \tag{2}$$

According to equation (2) *AUGER ELECTRON EMISSION* leads to a discrete electron energy in the δ-electron energy spectra; the *AUGER* electron energy only depends on the difference in the electron binding energies of the target atom. Table 1 shows excellent examples of *AUGER* electron energies for few light atoms up to Neon.

Since the target atom is practically at rest in the laboratory-system even after the collision, the discrete electron energies do not vary with the emission angle ϑ_e; the target *AUGER* electron is rather isotropic with respect to ϑ_e.

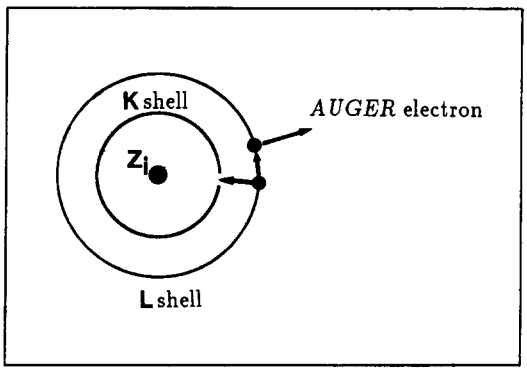

Fig. 5. Scheme of *AUGER* electron emission.

ELEMENT	*K-LL AUGER*, E_e [eV]
Li	45
Be	100
B	176
C	266
N	375
O	507
F	654
Ne	813

Tab. 1. *AUGER* electron energies for the first row elements.

Projectile electron emission

The energy distribution of emission process [4] (electron loss from the projectile) can be understood simply from a transformation of the velocity vectors of the projectile nucleus and its electrons from the laboratory-system to the centre of mass-system (*CMS*). In Figure 6 the velocity diagram shows the relevant vectors of the projectile ($\vec{v}_P$) and the ejected projectile electrons ($\vec{v}_{e,j}^{\,LS}$, $\vec{v}_{e,j}^{\,CMS}$). Since the projectile mass (m_P) is very large in comparison to the mass of the electron (m_e) the *CMS* is located in the moving projectile nucleus; its velocity vector v_{CMS} is identical with v_P in the *LS*.

In the *CMS* electrons produced by the *AUGER ELECTRON-* or the *ELECTRON LOSS PROCESS* are emitted with the velocity $\vec{v}_{e,j}^{\,CMS}$. By back transformation from the *CMS* to the *LS*, the velocity vector of the projectile loss electron ($\vec{v}_{e,j}^{\,LS}$) is obtained by summing up $\vec{v}_{e,j}^{\,CMS}$ and the velocity of the *CMS* (which is equal to $\vec{v}_P$, see above):

$$\vec{v}_{e,j}^{\,LS} = \vec{v}_{e,j}^{\,CMS} + \vec{v}_P \tag{3}$$

In the *CMS* the *AUGER-* and the *LOSS* electron energies differ by some order of magnitudes. Therefore, their angular dependence also differ strongly, as it will be seen below.

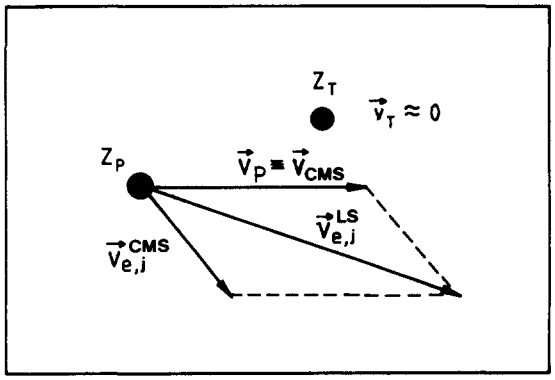

Fig. 6. Velocity diagram for the transformation from the centre of mass-system (*CMS*) to the laboratory system (*LS*). $\vec{v}^{LS}_{e,j}$ is the velocity in the *LS* and $\vec{v}^{CMS}_{e,j}$ the *CMS* velocity respectively. $\vec{v}_P$ is the projectile velocity, identical with the velocity of the centre of mass-system.

Projectile Auger electrons As it was mentioned above, *AUGER* electrons are emitted by autoionization, following vacancies in inner shells of ionized or multiply excited atoms. They appear as discrete lines in the δ-electron spectra, distributed isotropically in space. In the case of the moving projectile, in the laboratory-system the *AUGER* electrons are Doppler-shifted to higher energy values. This is due to summing up the velocity vector of the *AUGER* electrons $\vec{v}^{CMS}_{e,AUGER}$ and the velocity of the *CMS* ($\vec{v}_P$). For this reason the energy of the *PROJECTILE AUGER* electrons becomes a function of the emission angle $E_{e,AUGER}(\vartheta_e)$; the electron energy decreases with increasing emission angle. As was seen in Table 1, for inner shell vacancies the corresponding velocity $|\vec{v}^{CMS}_{e,AUGER}|$ can be equal or even larger than the projectile velocity $|\vec{v}_P|$. Consequently such δ-electrons can be observed at any, even backward, emission angles (ϑ_e).

Electron loss from the projectile In the *ELECTRON LOSS* process electrons with weak binding energy are ejected from the incident projectile by interaction with the target nucleus. This process is comparable with the *BE* (small impact parameter) and *TCEE* process (large impact parameter) explained above; but in the case of *LOSS* electrons the nucleus has to be considered in rest and the electrons as the incident collision partner.

For very large impact parameters the small momentum transfer from the target and projectile nucleus to the projectile electron leads to emission of electrons with low velocity ($\vec{v}^{CMS}_{e,loss}$) with respect to the projectile nucleus. With the condition ($|\vec{v}^{CMS}_{e,loss}| \ll |\vec{v}_P|$) and equation (3), the velocity of the *LOSS* electrons in the *LS* is calculated to be equal to the velocity of the projectile: $\vec{v}^{LS}_{e,loss} = \vec{v}_P$. In the energy spectrum these electrons appear as a cusp like peak around the energy:

$$E_{e,loss} = \frac{1}{2} m_e \vec{v}_P^2. \tag{4}$$

To lowest order the *LOSS* electrons may be considered to constitute a beam of electrons traveling with the incident beam in the forward direction ($\vartheta_e = 0^0$).

In the case of close collisions only the target nucleus and the projectile electron participate. Due to the simple classical two body collision the incident projectile electron is deviated at the target nucleus in all observation angles (ϑ_e). Depending on the impact parameter b_e, electrons emitted to forward angles relate to larger b_e, those from backward angles to smaller b_e. The emisson to $\vartheta_e = 180^0$ corresponds to the *KNOCK − ON COLLISION*. Since the mass ratio $\frac{m_e}{m_P}$ is very small the velocity of the *LOSS* electrons remains constant.

On the other hand, the intensity of this δ-electron peak decreases with increasing emission angles (ϑ_e) (see Figure 1). As it was mentioned above, the probability, i.e. the intensity of electron emission depends on the square of the impact parameter (b_e^2). Therefore, the greatest amount of *LOSS* electron emission in the *LS* is observed at large impact parameters respectively at small emission angles. Its minimum is reached at very close collisions, i.e. at backward angle $\vartheta_e = 180^0$.

ELECTRON PRODUCTION FROM HEAVY ION ATOM COLLISIONS

For lighter ions the electron emission follows nicely the expectations outlined above. For heavy ions (e.g. for Uranium) large deviations are observed. In Figure 7, for *1.4 MeV/u* U^{33+} on *Ar* the double differential δ-electron emission cross sections, $d^2\sigma/dE_e \cdot d\Omega_e$, are presented; in (a) the energy spectrum for the emission angle $\vartheta_e = 30^0$ and in (b) the angular distribution for the electron energy E_e=500eV is shown /5/. Of the collision processes [1] to [5], described above, only the two processes [1] and [2] are visible. The direct ionization of the target electrons is by far predominant all other reaction processes, (total ionization cross section $\sigma^I_{total} \approx 10^{-13} cm^2$). The "small" contribution of electron loss (process [5]) and *AUGER* electron emission (process [3] and [4]) are not visible in the energy spectra. In comparison to light ion atom collision the *BE* from heavy ion atom collision is strongly broadened.

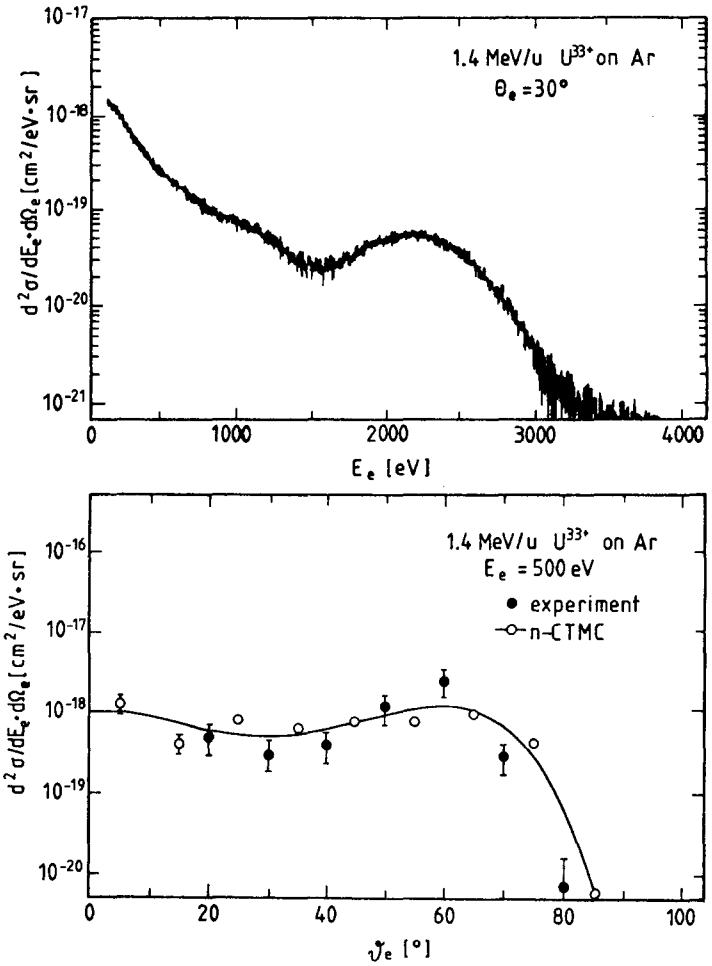

Fig. 7. (a) δ-electron energy dependence at $\vartheta_e = 30^0$ and
(b) angular dependence at E_e=500eV of double differential cross sections for $1.4 MeV/u\, U^{33+}$ on *Ar* (from /5/).

The most surprising result is, however, the extreme anisotropy in the angular distribution. Due to the strong two centre *COULOMB* force of the projectile and the target nuclei, the electron emission is strongly forward directed. Contrary to the observation for light ion impact, practically no electron is emitted into $\vartheta_e < 90^0$. According to *n-BODY CLASSICAL TRAJECTORY MONTE CARLO* calculations (*n-CTMC*) by Olson et al. [6], the target electronic states are strongly polarized in the two centre field and "focussed" by the *COULOMB* force into forward direction. Nearly 90% of all emitted electrons appear in a cone around $\vartheta_e \approx 60^0$. This anisotropic electron emission will lead to higher local energy deposition in the target material than expected for an isotropic electron emission. This may have an important effect on radiation damage of biological targets by heavy ion impact.

In Figure 8 the corresponding ionization cross section of Argon by Uranium impact as a function of the projectile energy (E_P) for different final charge states of the ionized target atoms, the so called recoil ions, (q) is shown /7/. Instead of single ionization now multiple ionization dominates and several simultanously emitted electrons are ejected. In more than 50% of all ionizing collisions multiple ionization dominates and the ionization cross section ($\sigma^I(q)$) decreases with increasing projectile energy (E_P) weaker than from the $1/E_P$ scaling law. Thus, higher order effects like polarization can no longer be neglected for heavy projectiles.

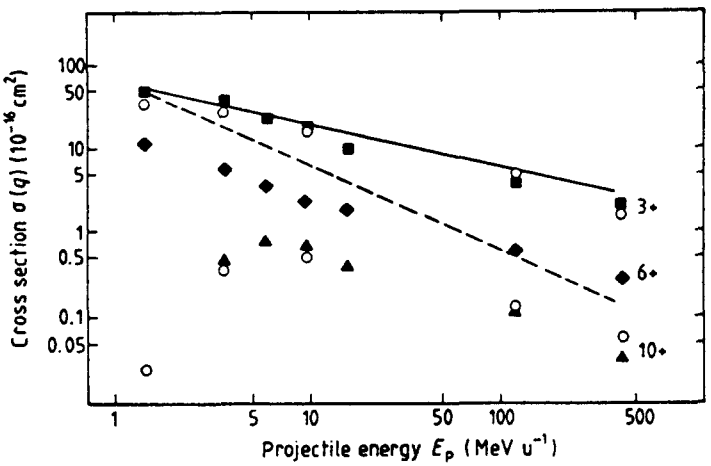

Fig.8 : Projectile energy E_e dependence of the multiple ionization cross section $\sigma(q)$ for Ar (the full symbols represent the measured data for $q = 3+, 6+, 10+$ and the open circles n-$CTMC$ values). The solid lines indicates the $1/v_P$, the dashed lines the $1/E_P$ dependence, respectively /7/.

In Figure 9 for $1.4\ MeV/u\ U^{33+}$ on Ar the differential energy loss cross section $\Delta S_e/\Delta E_e = E_e \cdot (\Delta\sigma_e/E_e)$, are presented /8/. The fraction ΔS_e represents the fractional energy loss transferred into kinetic energy of the emitted δ-electrons. For comparison, the corresponding proton data are shown /9/ (notice: factor 100 difference in absolut scale!). It is visible from these data, that at the same velocity for Uranium ions "hotter" δ-electrons are produced. In the case of proton impact on Ar most δ-electrons are produced around $E_e \approx 10eV$. For Uranium δ-electrons with an average kinetic energy around $100eV$ are emitted.

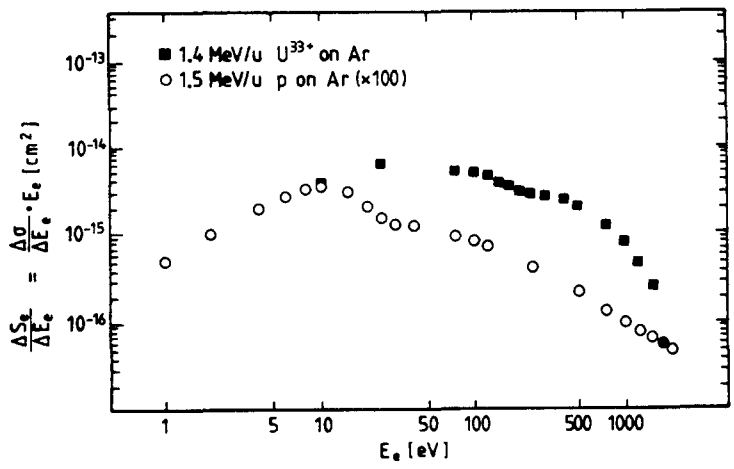

Fig.9 : Differential stopping power $\Delta S_e/\Delta E_e$ as a function of the δ-electron energy for protons and Uranium on Argon. The proton data are from Reference 9.

In Figure 10 the fractional energy loss, $\Delta S_I(q) = \Delta\sigma_I(q) \cdot E_I(q)$, is shown. This energy represents the energy loss transferred into pure ionization energy of the target atoms. $E_I(q)$ is the total ionization energy to excite q electrons just to the continuum with zero transational energy. The total electronic stopping power is given by summing up both: $\Delta S = \Delta S_I + \Delta S_e$. Again, the corresponding proton data from Reference 10 (multiplied with a factor 100) are shown in comparison. It can be seen, that for heavy ion impact a huge fraction of ΔS is indeed spent in multiple ionization processes.

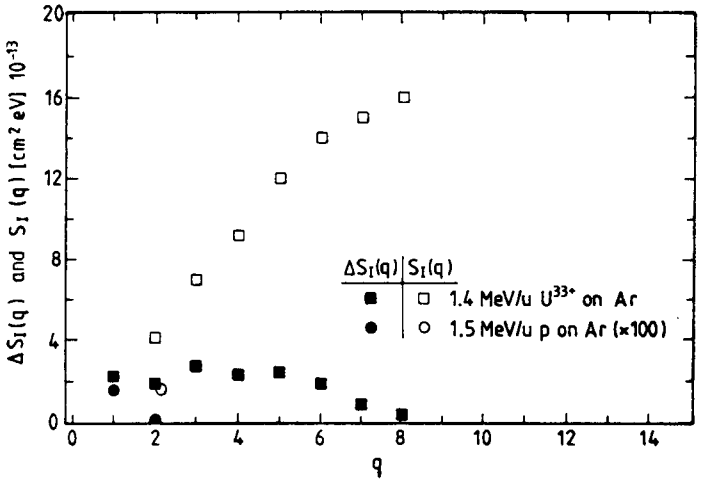

Fig. 10. Differential q-dependent energy loss $\Delta S_I(q)$ and $S_I(q)$ for *1.4 MeV/u* U^{33+} and *1.5 MeV/u* p on Ar, with $S_I(q) = \sum_{i=1}^{q} \Delta S_I(q_i)$ (from /8/, circles are proton data from /10/ multiplied by 100).

For light, fully stripped projectiles it is known that all differential electron emission cross sections scale with the square of the nuclear charge of the projectile (Z_P^2). Very recently Richard et al. /11/ and Quinteros et al. /12/ found experimentally, that for $\vartheta_e = 0^0$ the *BE* electron emission increases for decreasing projectile charge, if no fully stripped ions are considered. The investigation of those cross sections dependent on the initial and final projectile charge state indicated that the angular distribution of the electron emission is strongly dependent on the screening, i.e. on the projectile charge state. This is due to the stronger gradient of the screened projectile nuclear *COULOMB* force. The experimental observation are in good agreement with recent *n-CTMC* predictions by Olson et al. /13/. In contradictory to the q^2-scaling, Olson et al. calculated for U^{32+} on Ar at $\vartheta_e = 0^0$ *BE* emission cross section more than factor 10 higher than for U^{92+}. This again shows, that the two centre potential shape effects in heavy ion atom collisions has a strong influence on the δ-electron emission. The emission pattern in such collisions differs strongly from the light ion data. For heavy ion impact the relative *BE* contribution decreases and two centre effects, i.e. three and multiple particle momentum exchange, dominates.

At present only classical *n-CTMC* or n^2-*CTMC* models (Schulz et al. /14/) give a good discription of the δ-electron emission features. Fully quantum mechanical, many particle theories cannot describe at present the many particle processes. For radiobiological aspects, however, the *n-CTMC* models should give a sufficiently precise calculation of the differential cross sections.

REFERENCES

1. G. Kraft, Radiobiological Effects of very Heavy Ions: Inactivation, Induction of Chromosomal Aberrations and Strand Breaks, *Nucl.Science Appl.* 3, 1-28 (1987).
2. N. Stolterfoht and D. Schneider, Mechanisms for Electron Production in $30 - MeV\ O^{n+} + O_2$ Collisions, *Phys.Rev.* 33 , 59-62 (1974).
3. R.E. Olson, J. Ullrich and H. Schmidt-Böcking, Multiple-Ionization Collision Dynamics, *Phys.Rev.A* 39, 5572-5583 (1989).
4. F. Drepper and J.S. Brigg, Doubly Differential Cross Sections for Electron-Loss in Ion-Atom Collisions, *J.Phys.Rev.B: Atom.Molec.Phys.*, 2063-2071 (1976).
5. C. Kelbch, R.E. Olson, S. Schmidt, H. Schmidt-Böcking and S. Hagmann, Unexpected Angular Distribution of the δ-Electron Emission in $1.4\ MeV/u\ U^{33+}$-Rare-Gas Collision, *J.Phys.B: At.Mol.Opt.Phys* 22, 2171-2178 (1989).
6. R.E. Olson, Multiple-Ionization Cross Sections for Highly Stripped Ions Colliding with He, Ne and Ar, *J.Phys. B: Atom.Molec.Phys.* 12, 1843-1849 (1974).
7. H. Berg, R. Dörner, C. Kelbch, J. Ullrich, S. Hagmann, P. Richard, H. Schmidt-Böcking, A.S. Schlachter, M. Pior, H.J. Crawford, J.M. Engelage, I. Flores, D.H. Loyd, J. Pedersen and R.E. Olson, Multiple Ionization of Rare Gases by High-Energy Uranium Ions, *J.Phys.B: At.Mol.Opt.Phys* 21, 3929-3939 (1988).
8. S. Schmidt, Energie- Winkelabhängigkeit der δ-Elektronen- Emission in Stößen schneller Uranionen mit Edelgasen, *Diploma Thesis, University of Frankfurt* (1987).
9. M.E. Rudd, L.H. Toburen and N. Stolterfoht, Differential Cross Sections for Ejection Electrons from Argon by Protons, *At.Data Nucl. Data Tables* 23, 405-442 (1979).
10. R.B. Dubois and S.T. Manson, Multiple-Ionization Channels in Proton-Atom Collisions, *Phys.Rev.A* 35, 2007-2025 (1987)
11. P. Richard, D.H. Lee, T.J.M. Zoures, J.M. Sanders and J.L. Shinpauh, Anomalous Projectile Charge State Dependence of 0^0 Binary Encounter Electron Production in Energetic Collisions of F^{q+} *(q=3-6)* with *He* and H_2 Targets, *J.Phys.B: At.Mol.Opt.Phys* 23, ♯ 11, L213-l218 (1990).
12. T.B. Quinteros, A.D. Gonzales, O. Jagutzki, A. Skutlarz, D.H. Lee, S. Hagmann, P. Richard, S.L. Varghese and H. Schmidt-Böcking, Strong Projectile Charge State, *J.Phys.B: At.Mol.Opt.Phys*, in press (1990).
13. R.E. Olson, C.O. Reinhold and D.R. Schulz, Non-q^2 Scaling of the Ionization Cross Sections near the Binary Peak, *J.Phys.B: At.Mol.Opt.Phys* 23, ♯ 16, L455-L459 (1990).
14. D.R. Schulz, R.E. Olson, C.O. Reinhold, S. Kelbch, C. Kelbch, H. Schmidt-Böcking and J. Ullrich, Coincident Charge State Production in F^{6+} + *Ne* Collisions, *J.Phys.B: At.Mol.Opt.Phys*, in press (1990).